Supplement

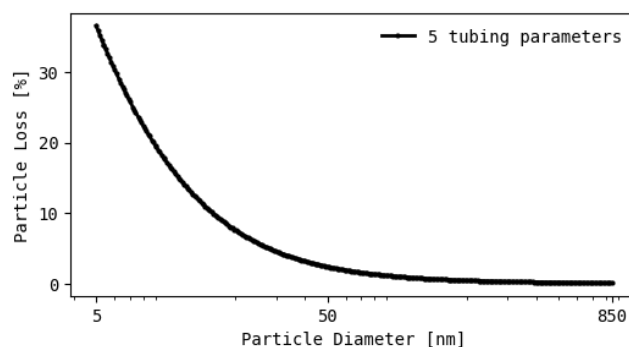**S1 Diffusional loss calculation for DMPS**

Fig S1: The particle loss from the whole-air inlet to the DMPS estimated using the Particle Loss Calculator (PLC) using a total of 5 tubing parameters (1. 22mm, 21LPM, 479cm, 2. 5.35mm, 6.3lpm, 138cm 3. 5.35mm, 3.8lpm, 13cm, 4. 5.35mm, 2lpm, 92cm, 5. 5.35mm, 1lpm, 51cm)

S2 Data screening and quality control

Here we describe the data screening and quality control procedure, describing the artefacts, comment on possible mechanisms and their frequency, and removal. We outline here two artefacts we removed when calculating the intensity parameter ($\Delta N_{max, 2.82-5}$) namely in-cloud events (S2.1) and windblown snow events (S2.2). We used visibility and wind speed measurements to help screen for these events. Visibility was used to ascertain whether the station was in-cloud, while the wind speed measurements were used to help identify windblown snow events. Isolating and removing these types of events was important when calculating the intensity parameter ($\Delta N_{max, 2.82-5}$), as we argue that in-cloud and wind-blown snow events should not be counted towards the production of nucleation mode particles via NPF.

S2.1 In-cloud events

When ZEP is submerged by dense clouds, there appears a sudden increase in the particle number concentration (~3-25nm, both polarities) as measured by the NAIS. The increase in number concentration is seen typically centred around 5nm. Furthermore, this is combined with a reduction in the concentration of both negative and positive ions. The increase in the particle concentration occurs when visibility dips below ~100m. We have labelled this type of occurrence as an in-cloud event (see an example of an in-cloud event on the 18th of August 2023, Fig S2). It was observed that the appearance of the 5nm mode was not dependent on the type of cloud (i.e. ice crystals compared with liquid water droplets using the Cloudnet data).

Fig S2: Example of an in-cloud event on the 2023-08-18 whereby a dense cloud submerges the observatory. The panels display (a) Cloudnet data, (b) ambient temperature, (c) visibility, (d) webcam, (e) NAIS measurements for the negative particles, (f) NAIS measurements for ions, (g) DMPS measurements, (h) wind speed and wind direction.

Fig S3: Arithmetic mean particle number size distributions (PNSDs) comparing out of cloud (red) and in-cloud (blue) for (a) NAIS measurements (negative particle channel), b) DMPS data, and c) Nano SMPS. The in-cloud and out of cloud conditions are selected based on visibility measurements collocated with PNSD measurements.

There is a substantial increase in the PNSD around 5nm for the NAIS data during in-cloud periods. Notice there is no increase around the 5nm mode for inside cloud measurements for both the DMPS and Nano SMPS PNSDs. Note that this is not showing the transition from in-cloud to cloud free conditions, but is the entire average for the PNSD measurements for each respective condition.

In the DMPS data, as opposed to NAIS measurements, we observe a distinct reduction in all particle sizes during in-cloud conditions when compared with out of cloud conditions (see Fig. S3 b) for average size distributions). In addition, the Nano-SMPS displays reductions within the size range of 3nm-20nm (see Fig. S3 c)). Both the DMPS system and Nano-SMPS display observations counter to that of the NAIS. For the NAIS there is a distinct increase around 5nm when we compared in-cloud with out of cloud data (see Fig. S3 a)). The differences between these sets of measurements suggests that when the NAIS measures during in-cloud conditions, some instrumental artefact leads to the observation that the number of small neutralised nucleation mode particles (around 5nm) increases. This cannot be explained by interstitial mode particles or the evaporation of cloud droplets (sampled and dried via the whole air inlet of the NAIS). We have to assume that this mode in the NAIS data generated by in-cloud conditions is an instrumental artefact. Moreover, we would typically expect for a reduction in the concentration of small nucleation mode particles due to the large sink effect resulting from large cloud droplets. The ion loss associated with cloud/fog formation, reported by Chen et al. (2017) is similar to the loss of ions during the observed in-cloud events at ZEP.

Size distributions of aerosol particles and ions have been measured in and out of cloud before (Lihavainen et al., 2007). Lihavainen et al. (2007) observed, during a whole day in which the observatory was in-cloud, there were no particles in the range 100-500nm, but a growing interstitial mode 20-30nm. They also observed an ion mode 10-40nm, originating from the coagulation of cluster ions. During a measurement period when the observatory transitioned from in-cloud to cloud free the 100-500nm mode reappeared potentially as a result of the evaporation of cloud droplets (i.e. residuals), and the cluster ion mode increased.

S2.2 Windblown snow events

In the NAIS measurements, we observe sudden increases in both ion and particle concentrations when wind speeds typically exceeded 10 ms^{-1} and the surface albedo was greater than 0.8, indicating a layer of snow on the ground (see an example of a windblown snow event on the 12th of December 2022, Fig S4). We term these types of events as windblown snow events. From the NAIS data, the increased ion concentrations, during windblown snow events are substantial for sizes around 1nm and 2-5nm; negligible increases are observed beyond sizes of 20nm (see Fig.

S5). During windblown snow events, increases in concentrations measured by the DMPS can be observed between 20-60nm (see Fig S5, DMPS 5-700nm), this is contrary to the NAIS measurements, which as stated before see no noticeable increase at sizes greater than 20nm. These windblown snow events are similar to the wind-induced ion formation reported by Chen et al. (2017).
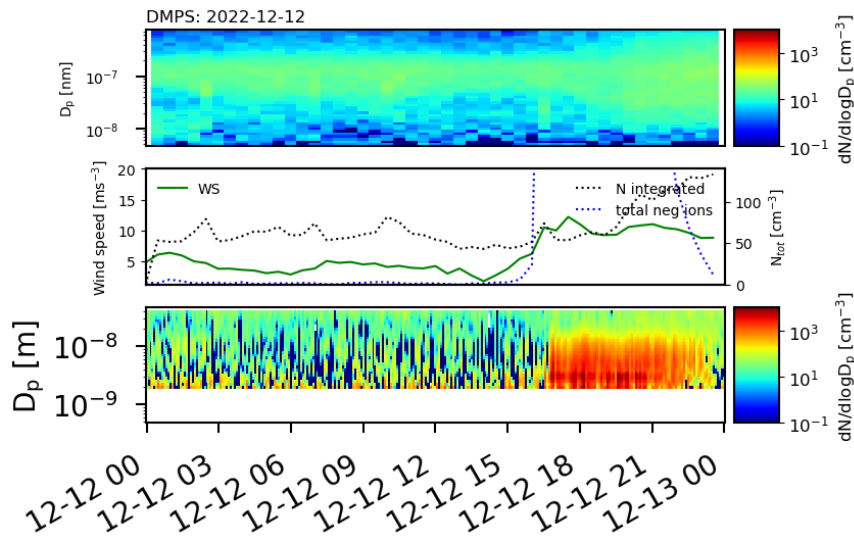

Fig S4: Example of windblown snow event on 2022-12-12 whereby the wind speeds increased above 10ms^{-1}, at 16:00 and a sustained burst of negative ions 1nm and larger could be observed. Panel (a) displays the particle number size distribution as measured by the DMPS, (b) shows the wind speed, concentration of total negative ions (dashed blue line), and total number as measured by the DMPS (dotted black line) (c) the ion number size distribution as measured by the NAIS (negative polarity).
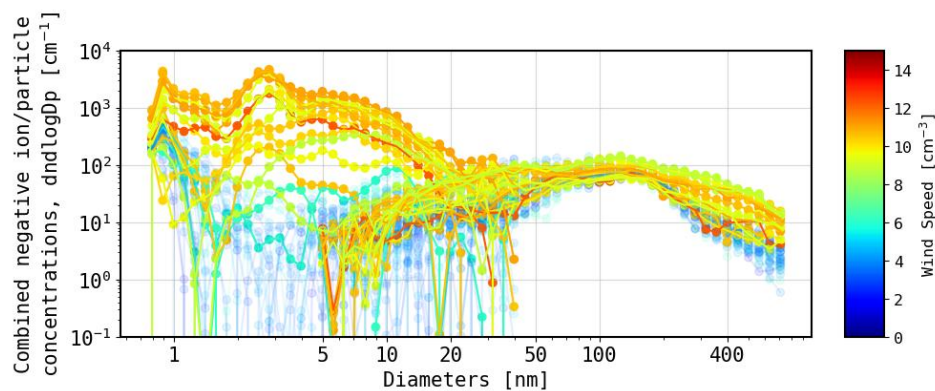
Fig S5: The negative ion concentration coloured by wind speed, and the DMPS particle number size concentration combined. Notice the log scale on the yaxis. The largest increase occurs beyond 10ms^{-1}. The increases in ion concentrations are most apparent at around 3nm, but are present from 1nm to 20nm. For the DMPS, wind speeds beyond 10ms^{-1} coincide with slight increased particle concentrations between 20nm to 50nm and beyond 200nm.

It is not clear whether these observations detail differing production mechanisms for ions and particles from blowing snow or whether it is an instrumental artefact related to the NAIS. The exact mechanism behind the increased concentrations in particles and ions and whether they constitute any climatic relevance remains unknown. Chen et al. (2017) suggested that these bursts in wind-induced ions are formed via the clustering of vapours released from resuspension processes, and that the shattering of resuspended snowflakes and ice particles by turbulence can lead to ions mostly below 7nm. For particles, the sublimation of blowing snow has been suggested to generate high concentrations of aerosol, potentially enhancing CCN concentrations and cloud properties (Gong et al., 2023). However, whether or not these ion bursts are relevant for the climate (i.e. are able to grow to sizes which can influence clouds (e.g. beyond 25nm) or interact substantially with light), needs to be seen.

S2.3 Frequency of occurrence
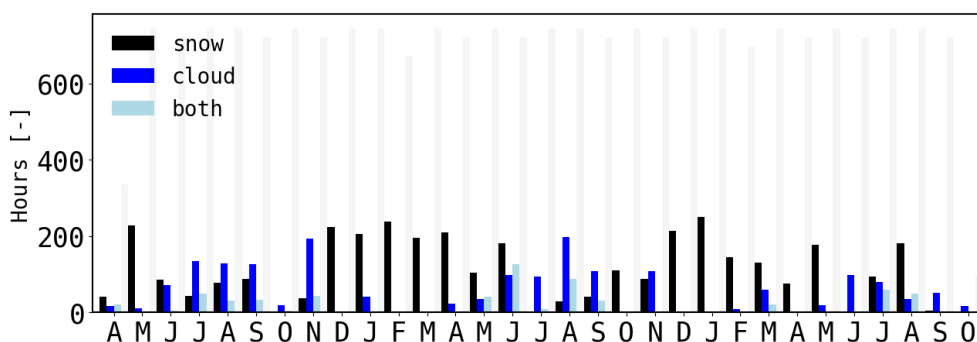
Fig S6: Number of hours of data (i.e. time steps) containing observed windblown snow periods. These are overlapping – improvement representation. Increased frequency of windblown snow events ('snow', black bar) in the winter and early spring. In-cloud events ('cloud', blue bars) increase in frequency in the summer months.

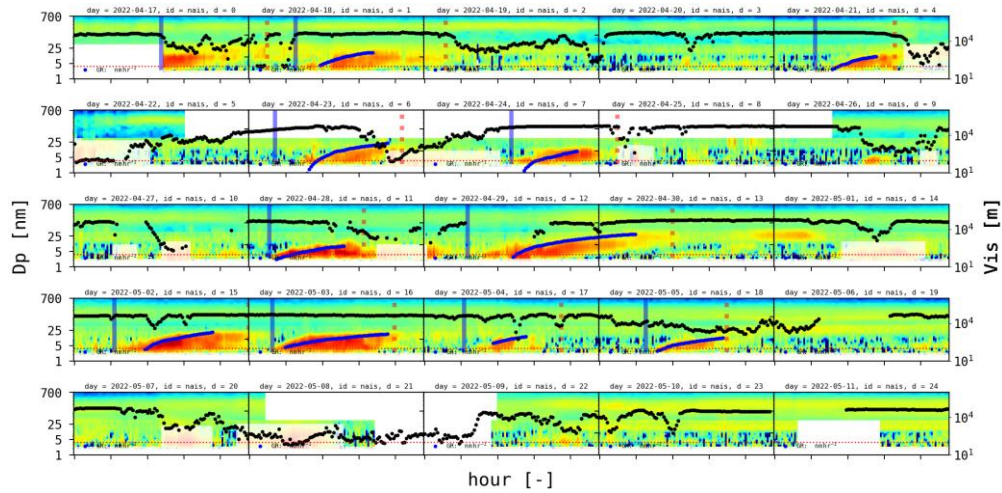**S2.4 Removal of in-cloud and windblown events**

Fig. S7: Consecutive days examining the particle number size distribution measured by the negative particle channel of the NAIS. Periods which experienced in-cloud events (i.e. sustained bursts of elevated particle number concentration typically in the 5nm mode during low visibility) and windblown snow events (i.e. sustained high ion number concentrations during wind speeds typically greater than 10ms^{-1}) are deselected (semi-transparent). The curve representing the growth of the nucleation mode that is used for the site of nucleation estimations is represented by the blue dots. The example of days presented are from 2023-04-27 to 2023-05-21.
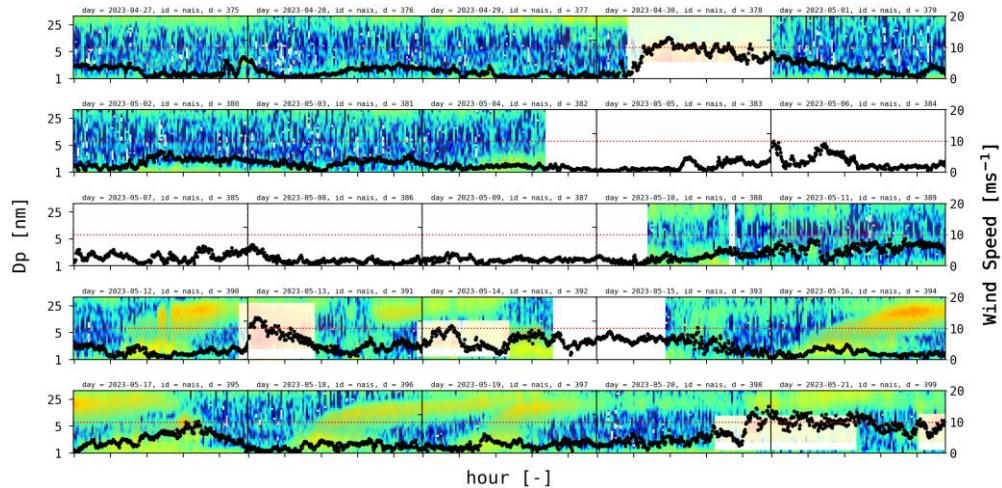
Fig. S8: Consecutive days examining the negative ion number size distribution measured by the NAIS. Periods which experience windblown snow events (i.e. sustained high ion number concentrations during wind speeds typically greater than 10ms^{-1}) are deselected (semi-transparent). The example of days presented are from 2023-04-27 to 2023-05-21.

S2.5 Comparison of NAIS and DMPS PSNDs

When comparing NAIS to DMPS/SMPS systems, the NAIS is often seen to overestimate concentrations. The problem is due to the multiple charge effect, where large particles are "given too much charge". NAIS can be expected to overestimate particle concentration by up to a factor of 10 compared to the DMPS (Kangasluoma et al., 2020). There are numerous papers which highlight this common discrepancy. Both the positive and negative NAIS measurements overestimate the particle number size distribution as measured by the DMPS. Currently, NAIS particle mode transfer functions need improving above 20nm.
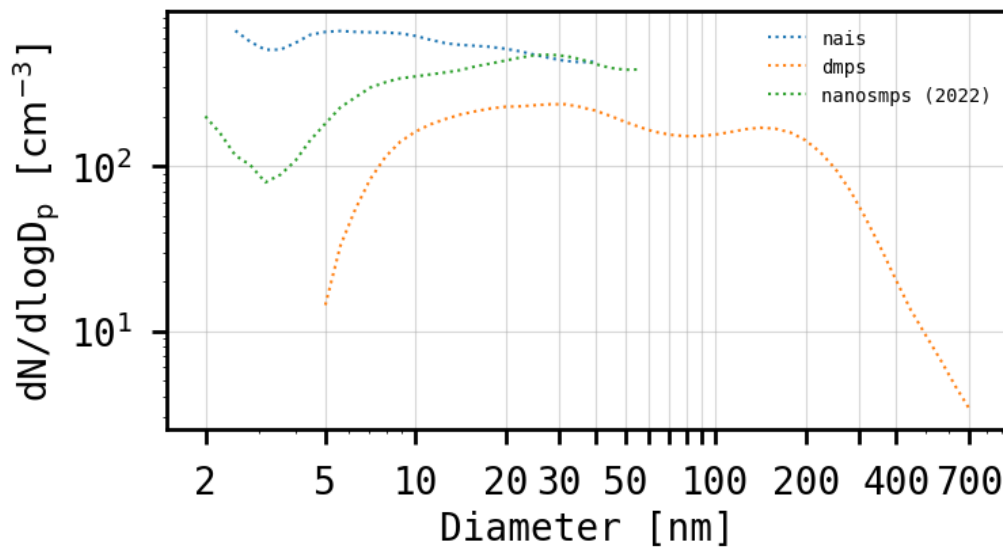
Fig S9: Particle number size concentrations for the NAIS, DMPS and Nano-SMPS.

Here we observe the seasonal dependence of the comparison between the NAIS and DMPS data. Notice that in summer and spring months (see Fig. X) the slope of the regression line is much closer to the 1:1 line, however, in autumn and winter the slope is around 0.2 (similar to the correction factor suggested by Dada et al., (2023)). Hence, when there is an increased number of nucleation mode particles, i.e. during the spring and summer season, the two instruments perform better.
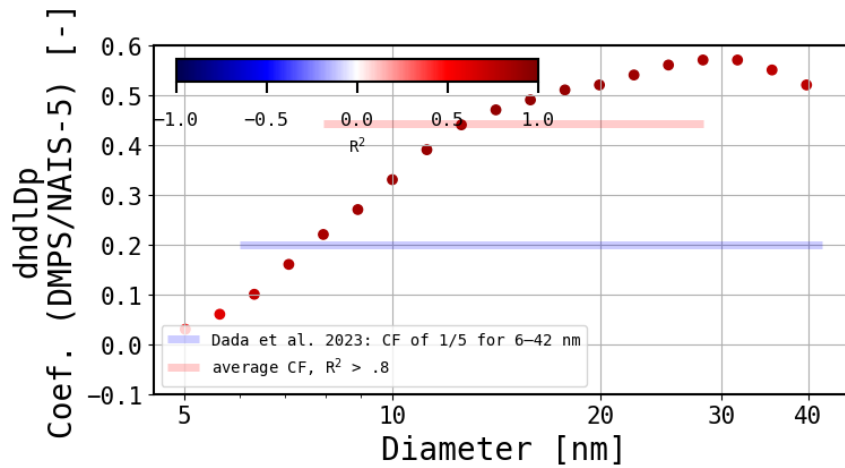
Fig S10: Dada et al., (2023) found that the NAIS overestimated the particle concentrations by a factor of 5 in the overlapping size range of 6–42 nm, and applied a correction factor of 1/5 to the NAIS measurements.
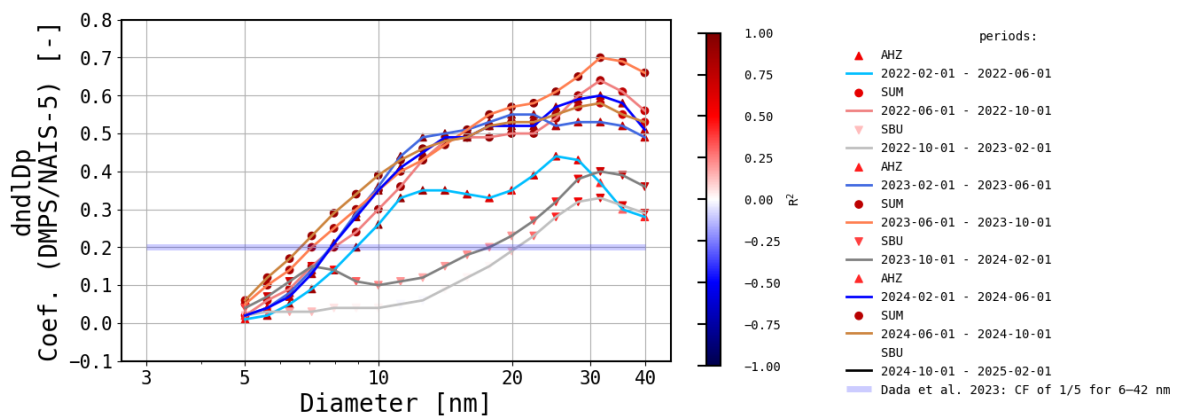

Fig S11: The regression line (i.e. slope) is on the y-axis and the diameter in which the comparison is performed is on the x-axis. For each comparison, the correlation of coefficient of calculated and is displayed by the colormap, red signifies a better correlation whilst blue a worse correlation.

S2.6 Loss of cluster ions

It should be noted that there is a reduced negative cluster ion mode apparent for the NIAS5 at ZEP; the exact reasons for this are unknown, but could be due to a build-up of dirt on the honeycomb mesh, the inlet, or the lack of proper grounding of the instrument. The negative cluster ions have the highest ion mobility and therefore most readily scavenged, hence the reduced concentration of the negative polarity compared with the positive.

S3 Nanoparticle ranking analysis

The nanoparticle ranking analysis utilised the daily maximum concentration of 2.82-5nm particles ($\Delta N_{max, 2.82-5}$) from the negative channel of the NAIS. $\Delta N_{max, 2.82-5}$ provided the best results when compared with the Dal Maso et al., (2005) classification. The nanoparticle ranking analysis developed by Aliaga et al. (2023) shows clear similarities with the classification performed in line with the Dal Maso et al., (2005) algorithm (see Fig. S12).
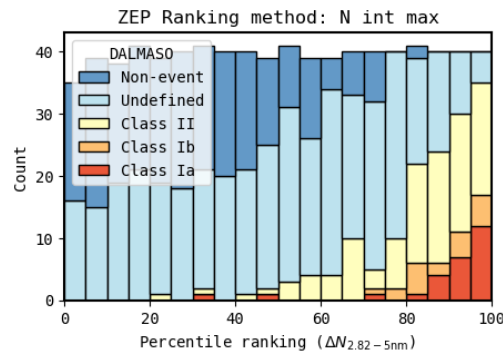

Fig S12: The results of the nanoparticle ranking analysis compared with the Dal Maso et al., (2005) classification: (a) the daily maximum for the total number concentration of 2.82 nm and 5 nm particles (N_{max}) is used as the intensity parameter to gauge the strength of the NPF day, in (b) the daily ratio of the 90th percentile and 20th percentile for the particle number concentration between 2.82 nm and 5 nm ($\Delta N_{2.82-5}$) corresponds to the strength of the atmospheric NPF event. N_{max} is more in agreement with the Dal Maso et al., (2005) classification, and hence prefered in this study. 90th percentile and 20th percentile The 90th/20th ratio of (i.e. 90th/20th ratio of $\Delta N_{2.82-5}$),
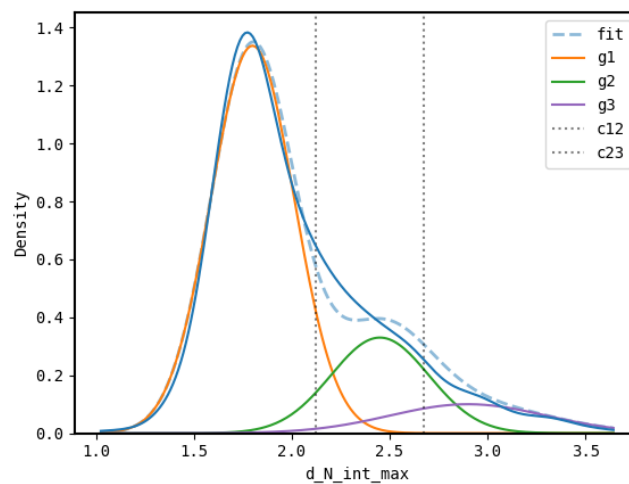
S3.1 Fitted classes for the Nanoranking anaylsis

Fig S13: Fitting for the intensity parameter. Note that the mapping used between dNint,max and the class of event i.e. g1, g2 g3 is 1:1. The fitting groups the days based on log of the strength parameter.
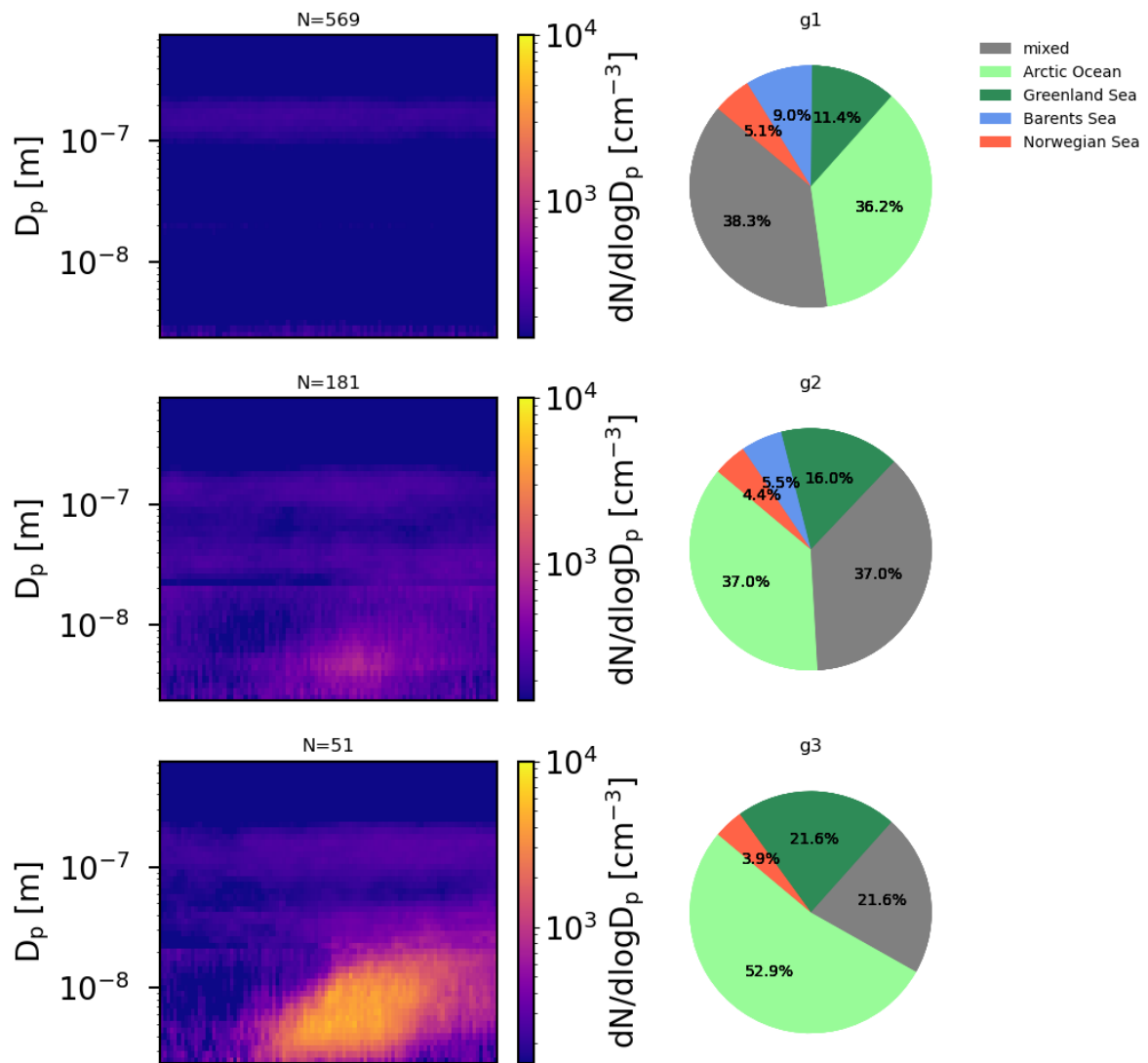
Fig S14: Using the nanoranking we divided the days in three classificaitons using a pdf fitting on the intensity parameter. Barents is linked to very few events. The Arctic Ocean covers the majority of NPF. You can see the fit in the supplement. In total about 51 g3s, 181 g2s and 569 g1.
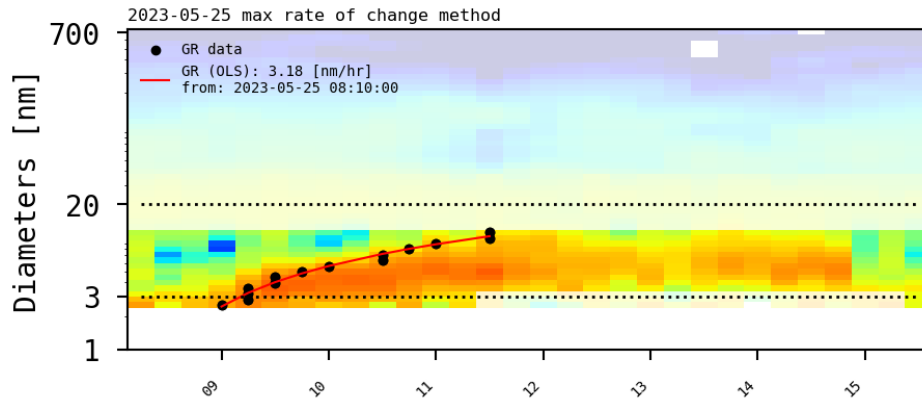
S4 Calculation of growth rates

Fig S15: Example event day (2023-05-25) with growth rate (GR) calculations. The slightly translucent areas display the data which is not used in the calculation. The rate of change method is used to find the datetime at which an individual size bin (Dp) experiences the largest increase in number concentration; for each Dp the time at which this occurs is displayed by the black dot. The red curve is the ordinary least squares method (OLS) providing a linear fit. GR is the gradient of the red curve.

S5 Polar night events

The polar night events include the following:

1. 2022-11-25 20:00 - 2022-11-26 15:00, **2.** 2023-10-25 20:00 - 2023-10-26 23:50, **3ab.** 2023-10-28 (x2, 01:00 12:00) – 2023-10-29 15:00, **4.** 2023-11-01 09:00 - 2023-11-02 18:00, **5.** 2023-11-02 21:00 -2023-11-03 06:00.
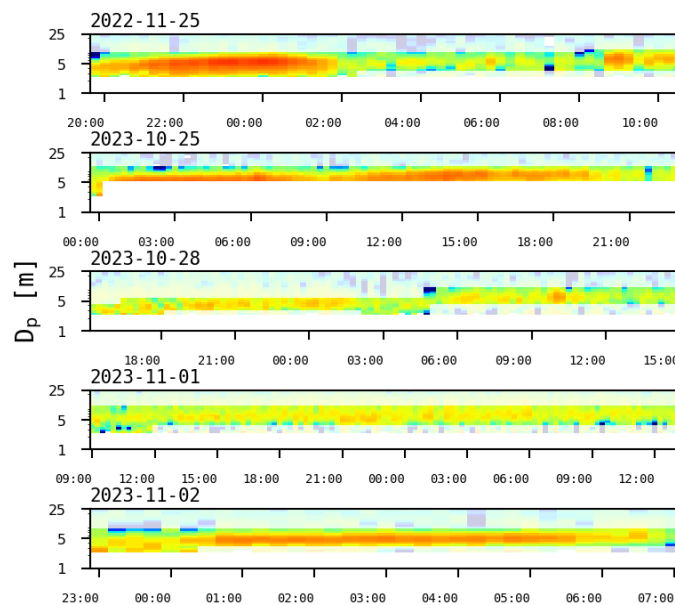
Fig S16: Particle number size distribution surface plots for the polar night events.

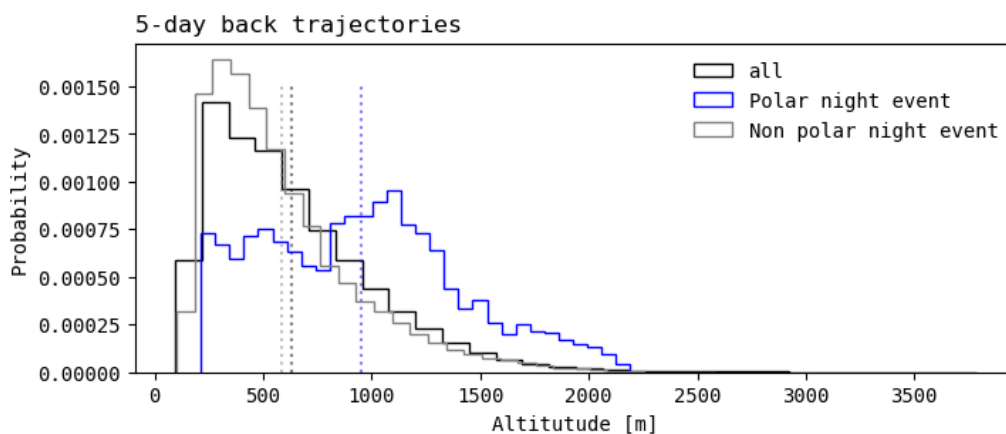## S5.1 Altitude of all polar night events

Fig S17: Histogram for the altitudes of all the endpoints that make up the 5-day back trajectories, comparing all NPF events not during the polar day and all the polar night events (defined as events after the 26th of October).
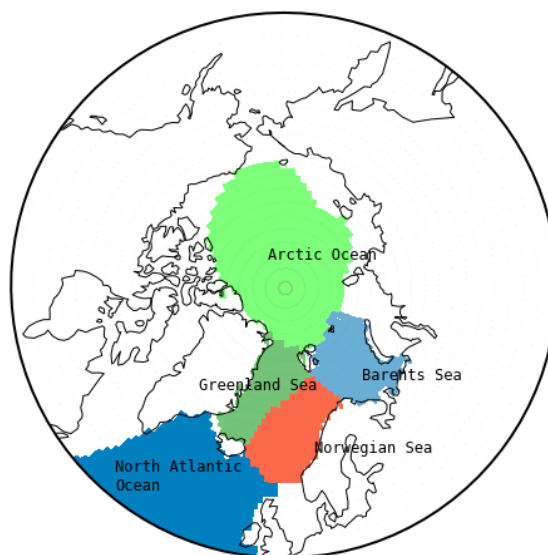
S6 Marine air mass sectors

Fig S18: The definitions for the marine air mass sectors based on marine domains. Using the marine areas / Ocean basins outlined in https://regionmask.readthedocs.io/en/stable/defined_ocean_basins.html and obtained by Natural Earth https://www.naturalearthdata.com/